

URTeC: 4053742

Interference Testing in Shale: A Generalized ‘Degree of Production Interference’ (DPI) and Developing New Insights into the Chow Pressure Group (CPG)

Chris Ponnors¹, Mohsen Babazadeh², Craig Cipolla³, Karan Dhuldhoya², Qin Lu², Ripudaman Manchanda⁴, Daniel Ramirez Tamayo⁴, Steve Smith⁴, Mojtaba Shahri⁵, Mark McClure¹; 1. ResFrac Corporation, 2. ConocoPhillips Company, 3. Hess Corporation, 4. Exxon Mobil Corporation, 5. Apache Corporation

Copyright 2024, Unconventional Resources Technology Conference (URTeC) DOI 10.15530/urtec-2024-4053742

This paper was prepared for presentation at the Unconventional Resources Technology Conference held in Houston, Texas, USA, 17-19 June 2024.

The URTeC Technical Program Committee accepted this presentation on the basis of information contained in an abstract submitted by the author(s). The contents of this paper have not been reviewed by URTeC and URTeC does not warrant the accuracy, reliability, or timeliness of any information herein. All information is the responsibility of, and, is subject to corrections by the author(s). Any person or entity that relies on any information obtained from this paper does so at their own risk. The information herein does not necessarily reflect any position of URTeC. Any reproduction, distribution, or storage of any part of this paper by anyone other than the author without the written consent of URTeC is prohibited.

Abstract

This study integrates field data, numerical simulations, and analytical derivations to study production interference testing in shale. First, we investigate the Chow Pressure Group (CPG) technique, and: (a) explain why the CPG has a qualitative association with the strength of production interference, (b) assess the conditions under which the CPG reaches a stable long-term plateau during the typical duration of a test, and (c) if it does, explain whether this plateau has a physical interpretation. Next, we study the Devon Quantification of Interference (DQI) technique, and: (a) use the ‘two-well’ Degree of Production Interference (DPI) metric to derive a relationship for a ‘uniform-spacing’ DPI that is applicable for a well bounded on both sides, and (b) develop a procedure to calculate a generalized DPI that accounts for arbitrary gun-barrel configurations, spatially variable fracture conductivity, and anisotropy. The new generalized DPI technique is validated by applying to a field dataset where extended shut-ins (2+ days) were performed months after the interference tests, allowing independent assessment of the interference test interpretations. The generalized DPI procedure: (a) provides fracture conductivity measurements that can be used in general-purpose reservoir engineering calculations, and (b) enables rapid ‘what-if’ analysis to test the economic impact of modifying well configuration.

1. Introduction

Interference tests are used to inform well spacing decisions in shale. When a well is put on production, pressure is measured in one or more offset wells and analyzed to assess the strength of the hydraulic connection. If tests are performed at different distances, it is possible to estimate the relationship between spacing and connectivity.

The Chow Pressure Group (CPG) technique is commonly used to interpret interference tests. The CPG is a metric related to the power-law scaling of ΔP (the pressure change caused by the offset production) with respect to time. The CPG concept first was applied to rate-transient analysis (RTA) by Chu et al. (2017) as an empirical way of describing trends that exhibit deviation from linear flow. Subsequently, Chu et al. (2020) showed that the CPG metric can be applied to analyze interference tests. Lower values of CPG (0-0.4) indicate weak interference and higher values (greater than 0.7) indicate strong interference.

Almasoodi et al. (2023) introduced the ‘Devon Quantification of Interference’ (DQI) method. In this procedure, the initial pressure response at the monitoring well is matched with the solution to the 1D diffusivity equation, as observed from an offset location. The match is used to estimate hydraulic diffusivity, which is then used to calculate fracture conductivity. Finally, the conductivity is used to estimate the ‘degree of production interference’ (DPI), a metric that quantifies the amount of production loss at the monitoring well caused by the offset well.

In this study, we integrate numerical simulations and field data to address several questions related to CPG and DQI procedures:

- a. The CPG metric has a qualitative relationship with production interference. What is the theoretical basis for this relationship?
- b. Simulations from Almasoodi et al. (2023) predict a loose relationship between CPG and DPI. If we look across a population of actual field interference tests, will this relationship be apparent, and with how much scatter?
- c. Many interference tests appear to exhibit a plateauing of CPG at a stable value. Is this plateau physically meaningful, and if so, how should it be interpreted?
- d. Almasoodi et al. (2023) derived a metric to estimate production interference for a ‘two-well’ system, with the wells unbounded on the outside. Can we generalize this procedure to estimate the degree of production interference for uniform spacing or arbitrary gun-barrel configurations? How do we account for spatial variability in fracture conductivity?

2. Theory and/or Methods

2.1 Generic example of an interference test

Figure 1 shows a schematic of a typical interference test. The production well (dashed lines) is put on production, causing a delayed and attenuated pressure response in the monitoring well (solid line). After a few days, the monitoring well is also put on production.

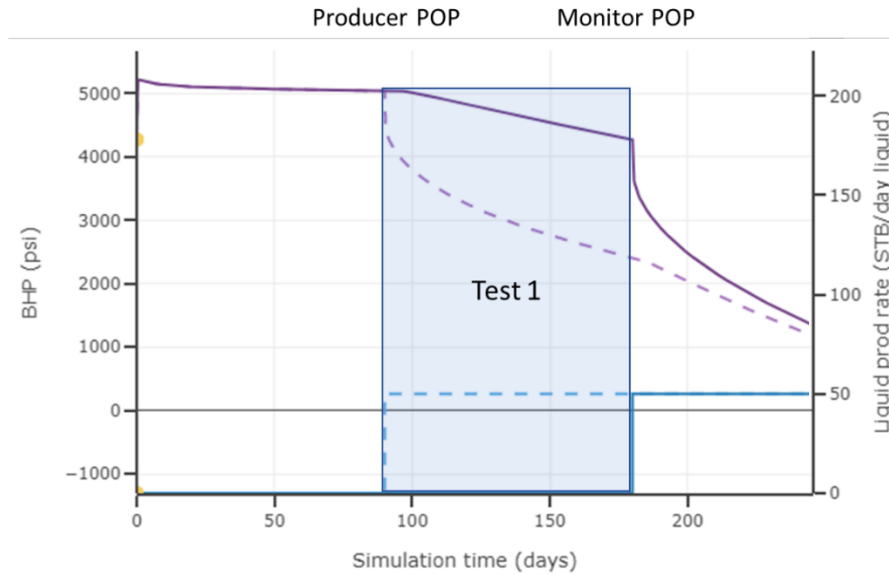


Figure 1: Schematic of an interference test. The dashed lines show rate and pressure for the production well, and the solid lines show the pressure and rate for the monitoring well. The monitoring well is put on production a few days after the production well.

2.2 Bourdet derivative and CPG plots

Figure 2 shows results from a numerical simulation of an interference test. The left panel shows pressure in the monitoring well before and after the start of production in the offset well (marked with the vertical black line). The green line shows the extrapolation of the trend from prior to the start of the test. ΔP is calculated by taking the difference between the green and red lines. The right panel of Figure 2 shows ΔP , $\Delta P'$, and CPG plotted on a loglog plot (defined below). Typically, interference tests are performed for only a few days. However, this simulation extends to more than 10,000 hours (more than 416 days).

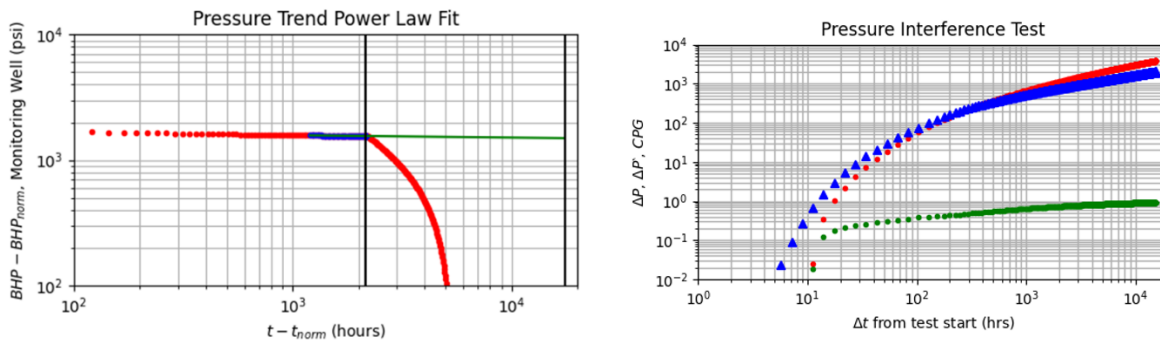


Figure 2: Pressure versus time before and during an interference test (left) and a loglog plot of dP , dP' , and CPG during the test (right).

The Bourdet derivative $\Delta P'$ is defined as:

$$\Delta P' = t \frac{d\Delta P}{dt} = \frac{d\Delta P}{d(\ln(t))}, \quad (1)$$

where t , time, is measured from the beginning of production.

The CPG metric is defined as (Chu et al., 2017; 2020):

$$CPG = \frac{\Delta P}{2\Delta P'}. \quad (2)$$

In many situations, ΔP appears to follow a power-law scaling with time:

$$\Delta P = At^a, \quad (3)$$

where a and A are constants.

The loglog slope of $\Delta P'$ is equal to a , because:

$$t \frac{d\Delta P}{dt} = Aat^a, \quad (4)$$

$$\ln(Aat^a) = \ln(A) + \ln(a) + a\ln(t), \quad (5)$$

$$\frac{d(\ln(A)+\ln(a)+a\ln(t))}{d(\ln(t))} = a. \quad (6)$$

This property suggests an alternative definition for CPG:

$$CPG = \frac{1}{2a}. \quad (7)$$

For linear flow, ΔP scales with the square root of time, so a is equal to 1/2, and CPG is equal to 1.0. For ‘boundary dominated’ flow, ΔP scales linearly with time, and so CPG is equal to 1/2.

CPG values are a necessary, but not sufficient condition to diagnose flow regime. In other words, if CPG is equal to 1/2, this does not necessarily prove that flow is in a ‘boundary dominated’ regime; and if CPG is 1.0, this does not necessarily prove that flow is in a linear flow regime.

When applied to rate-transient analysis, a value of a greater than 1/2 (CPG less than 1.0) indicates deviation from linear flow, and consequently, more-rapid pressure drawdown than would be expected from standard linear flow (or more precisely, a less rapidly decreasing rate of drawdown). Deviation from linear flow is a common observation in shale (Chu et al., 2017; Figure 20 from McClure et al., 2023a).

When applied to interference test analysis, it may seem counterintuitive that a lower CPG value indicates a *weaker* connection, since lower CPG implies a larger value of a and so, a *more rapid* rate of pressure change. This surprising result is explained in Section 3.1.

2.3 DQI method of interpretation

The DQI method starts by performing a curve-fit to the initial pressure response at the monitoring well. The fit provides an estimate for the hydraulic diffusivity. Observed from an offset position, the 1D diffusivity equation is:

$$P(y, t) - P(y, 0) = \frac{2q_0\sqrt{\alpha t}}{K} \exp\left(-\frac{y^2}{4\alpha t}\right) - \frac{q_0 y}{K} \operatorname{erfc}\left(\frac{y}{2\sqrt{\alpha t}}\right), \quad (8)$$

where q_0 is the production rate per fracture (in reservoir volume, not surface volume), y is the offset distance, α is the hydraulic diffusivity, and K is a lumped parameter. The measured pressure transient can be matched by varying the parameters K and α . They are defined as:

$$\alpha = \frac{k_f W}{\mu \left(\frac{dW}{dP} + c_f W\right)} = \frac{C}{\mu \left(\frac{dW}{dP} + c_f W\right)}, \quad (9)$$

$$K = \frac{CH}{\mu}, \quad (10)$$

where C is fracture conductivity, k_f is fracture conductivity, W is fracture aperture, c_f is the fluid compressibility, μ is the fluid viscosity, and H is the fracture height.

The objective of the curve fit is to estimate the hydraulic diffusivity, α . The hydraulic diffusivity is used to estimate the fracture conductivity by plugging into Equation 9. The value K is not used to estimate any parameters; it is used solely to facilitate the curve fit. When applying Equation 9, the fluid compressibility and viscosity should be estimated from the *fluid in the fracture during the test*. The values of fracture aperture and its derivative, W and $\frac{dW}{dP}$, can be assumed to be 0.03 inches and a range of 2e-6 to 8e-6 inches/psi, which are reasonable estimates for propped fractures (Almasoodi et al., 2023).

To calculate q_0 , the total wellhead flow rate must be converted to reservoir volumes and divided by the number of flowing fractures along the well. The number of flowing fractures along the well is not known with confidence. Fortunately, the value of q_0 affects only the value of K , not the value of α , and the key results of the analysis depend on α , not K . For a reasonable estimate, it may be assumed that the ‘number of flowing fractures’ is equal to the number of perforation clusters, multiplied by an assumed efficiency, such as 75% (Benish et al., 2024). In a well with openhole completion, it is reasonable to assume one flowing fracture per stage (Craig et al., 2021).

Matching the full pressure transient with a mathematical solution would be complex and nonunique because of uncertainty in the geometry of the various flowing fractures connected to the wells. To avoid this problem, the method focuses solely on matching the *initial* pressure response at the monitoring well, which depends on only hydraulic diffusivity, and is not affected by uncertainties in flow geometry, K , drawdown rate at the production well, or any other parameter. This is because the expression for ‘radius of investigation’ during a pressure transient is:

$$r_{inv} = 4\sqrt{\alpha t}. \quad (11)$$

In other words, the initial response to production – as observed from an offset observation point – is affected solely by the hydraulic diffusivity, distance, and time.

Once conductivity has been estimated, Almasoodi et al. (2023) provide a procedure for estimating the ‘degree of production interference,’ defined as:

$$DPI = \frac{q_{20days} - q_{bef}}{q_{bef}}, \quad (12)$$

where q_{bef} is the production rate of one of the wells when both wells are producing, and q_{20days} is the flow rate that would be observed 20 days after one of the wells is shut-in. The duration ‘20 days’ is arbitrary, and the DPI may be more generally interpreted as representing the production impact over the long-term, after transient effects have stabilized.

A DPI of 1.0 corresponds to a doubling of the production rate with the shut-in of the offset well. For two wells (unbounded on the outside), the DPI cannot be greater than 1.0 because an adjacent well can only impact production on one side of its neighbor.

Almasoodi et al. (2023) showed that the relationship between fracture conductivity and DPI depends on the relative strength of formation deliverability into the fracture and the fracture's ability to transport fluid toward the well. Based on this concept, it is possible to calculate a ‘dimensionless drainage length,’ L_D , and then relate this quantity to the DPI (Appendix A).

The DPI expression derived by Almasoodi et al. (2023) is only valid for a specific configuration – two wells unbounded on either side with symmetric fracture geometries. It is convenient to call this metric the ‘two-well DPI.’ In Appendix B, we derive an expression for a different configuration – a well bounded on both sides with uniform spacing. This metric can be defined as the ‘uniform-spacing DPI.’ In Section 2.4, we develop a procedure for calculating a generalized DPI for arbitrary gun-barrel configurations.

It is useful to define the fractional production loss from production interference (FPL):

$$FPL = 1 - \frac{q_{bounded}}{q_{unbounded}}, \quad (13)$$

where $q_{unbounded}$ is the production rate that the well would have had if unbounded by one or more neighbors, and $q_{bounded}$ is the flow rate in the bounded configuration. The value of q_{bef}/q_{20days} is approximately equivalent to $q_{bounded}/q_{unbounded}$, and so we can write:

$$FPL = \frac{DPI}{DPI+1}, \quad (14)$$

Or equivalently:

$$DPI = \frac{FPL}{1-FPL}. \quad (15)$$

For example, a DPI of 1.0 corresponds to FPL of 0.5 – a 50% reduction in production due to interference from the neighboring well. When a well is bounded on either side, it is possible for the value of FPL to be greater than 0.5, corresponding to DPI greater than 1.0.

The metrics DPI and FPL can be estimated for a variety of different configurations. For example, they can be used to quantify the effect of removing one other neighboring well. Alternatively, they can be used to quantify the effect of removing all neighboring wells.

2.4 Generalized DPI for arbitrary gun-barrel configurations

The Generalized DPI procedure combines results from multiple interference tests to estimate the effect of changing well spacing/configuration, while accounting well-to-well interference in arbitrary gun-barrel configurations and heterogeneity of fracture conductivity.

The method starts by assigning a ‘maximum-possible drainage volume’ to each well. The maximum extent of the depletion region around each well can be approximated with a Voronoi diagram (Kim, 2019). The Voronoi diagram assigns each location in the drainage region to the closest depleting fracture (Figure 3). To prevent production ‘out of zone,’ the user specifies the depth interval(s) of the pay zones accessed by the wells. As known from classical well test analysis, the boundaries between the Voronoi regions are equivalent to no-flow boundary conditions (Horne, 1995). If the proppant pack conductivity is anisotropic, the Voronoi diagram can be generated using ellipses, rather than circles (Figure 4). If the ratio of horizontal to vertical conductivity is C_h/C_v , then the long axis will be $\sqrt{C_h/C_v}$ longer than the short axis. There is a ‘square root’ scaling with anisotropy because the ‘radius of investigation’ scales with the square root of hydraulic diffusivity.

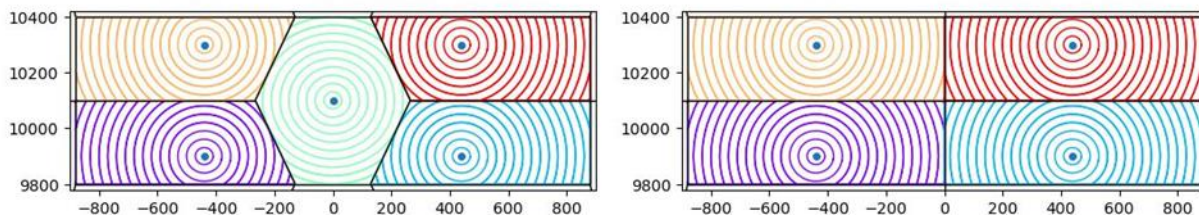


Figure 3: Visualization of depletion regions around wells with a four and five-well gun-barrel configuration.

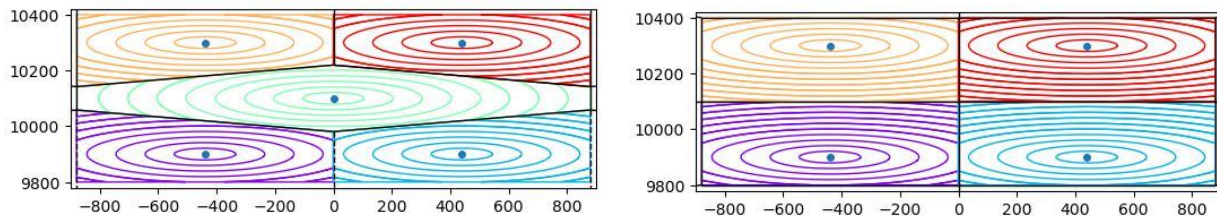


Figure 4: Visualization of depletion regions around wells with a four and five-well gun-barrel configurations, assuming 25x conductivity anisotropy.

Next, results from multiple tests are aggregated to estimate the distribution of conductivity along fracture strike. Projects with offset pressure observation laterals demonstrate that a spatial gradient develops along the producing fractures, with the lowest pressure near the well (Cipolla et al., 2022; Liang et al., 2022; Benish et al., 2024). These observations are concordant with the conductivity estimates coming from interference tests, which imply that proppant packs during depletion are not effectively infinite conductivity. The consequence of finite fracture conductivity is that the pressure drawdown and productivity diminish with distance.

Because proppant settles and is held-up during propagation, fracture conductivity decreases with distance (Liang et al., 2022; Benish et al., 2024). For example, Figure 5 shows results from a set of interference tests performed in the Bakken and Three Forks. Each dot represents an individual test between an active well and a monitor well. To estimate conductivity versus distance, tests can be aggregated from wells within reasonable spatial proximity to each other and with similar fracturing designs, so that they can be considered ‘comparable.’ The light blue curves show empirical matches to the data with Gaussian curves.

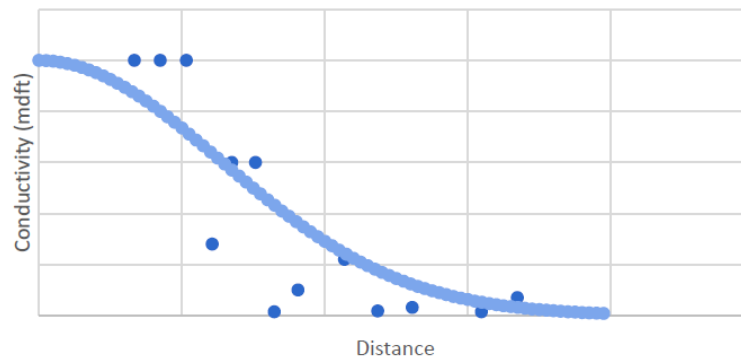


Figure 5: Empirical measurements of fracture conductivity versus distance from a series of interference tests performed in the Bakken and Three Forks. Each dot represents a particular interference test.

Figure 6 shows results from a series of interference tests in the Midland Basin. In this case, a direct plot of conductivity (estimated from the DQI procedure described in Section 2.3) versus distance (left panel) shows a weak trend with distance. However, the wells are staggered across two different landing depths. Interference between wells in different zones tends to be weaker than would be expected if conductivity was assumed to be isotropic. As shown in the right panel, the trend can be improved if we assume a 5x ratio between the horizontal and vertical conductivities. Appendix C shows how the DPI conductivity estimate from the DQI method can be adjusted to account for anisotropy.

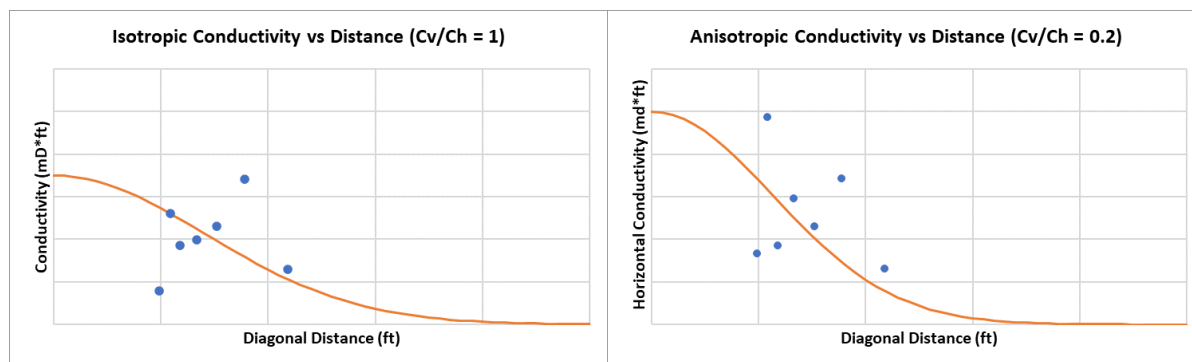


Figure 6: Empirical measurements of fracture conductivity versus distance from a series of interference tests performed in the Midland Basin. Each dot represents a particular interference test. The panel on the right assumes vertical conductivity is 5x lower than horizontal conductivity.

Figure 6 shows estimated conductivity (from the DQI method) versus distance. Because conductivity is not spatially uniform along the fracture, the measured (i.e., estimated) conductivity curve is not the same thing as the *actual* conductivity versus distance curve. The measured conductivity from the interference test should be equal to the harmonic average of the actual conductivity distribution between the wells.

To illustrate, Figure 7 shows a hypothetical scenario with two wells 880 ft apart and a DQI-estimated conductivity of 16 md-ft. Conductivity is assumed to be isotropic. As illustrated in the left panels, conductivity is greatest at the wells and diminishes with distance. The horizontal green line in the upper left panel shows the measured conductivity of 16 md-ft between the two wells. It is the distance-weighted harmonic average of the fracture conductivity distribution along a line between the two wells. Because proppant is placed in the vicinity of *both* wells, the *measured* conductivity diminishes more slowly with

distance than the *actual* conductivity. The right panel of Figure 7 shows the measured conductivity in green, and the implied actual conductivity versus distance in blue. The ‘actual conductivity’ curve is back-calculated from the ‘measured conductivity’ curve from the assumption that the measured conductivity is the harmonic average the ‘actual’ conductivity distribution between the wells.

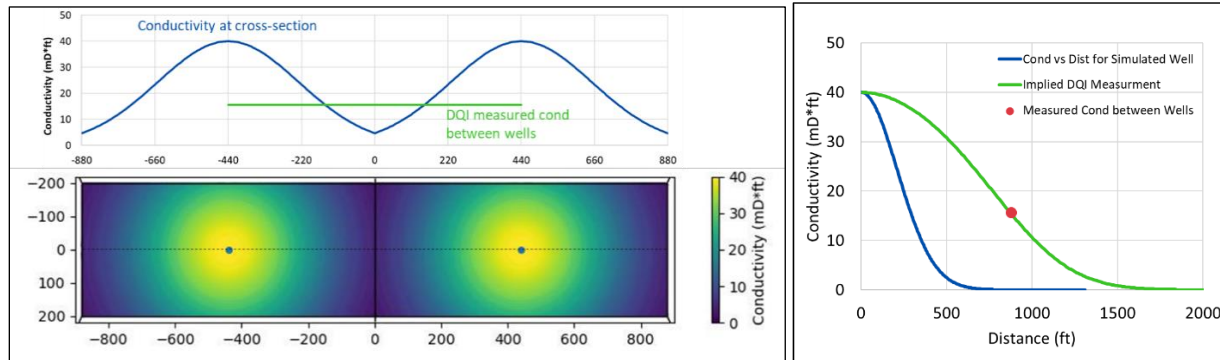


Figure 7: Left – Gun-barrel heat map of conductivity distribution for hypothetical isotropic two-well setup and conductivity vs x-location cross-section at the well depths. Right – Conductivity vs distance relationship (blue) required to match DQI measured conductivity vs well spacing (green).

Based on these concepts, we propose a fast-running, semianalytic procedure for estimating DPI and FPL for arbitrary gun-barrel configurations. We radially discretize around each well, as shown in Figure 8. If the radial discretization hits the edge of the depletion region – either because it has reached the edge of the drainage region determined from the Voronoi diagram, or because it has reached the edge of the overall bounding box defined by the user, then that part of the radius is not included.

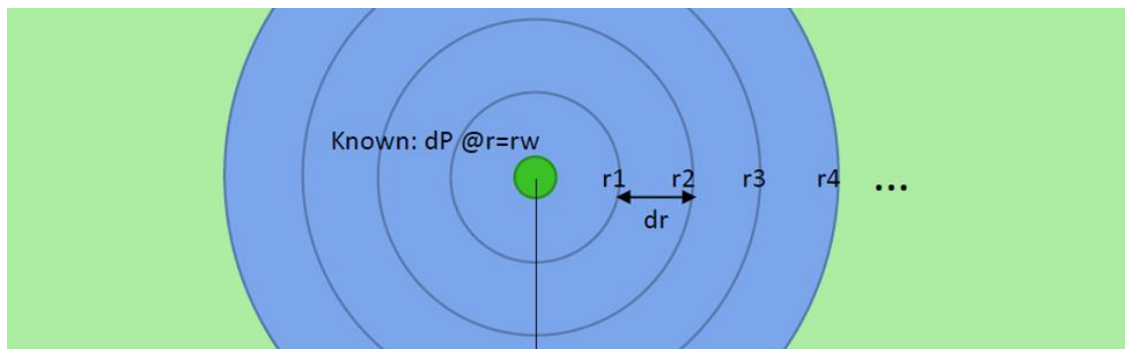


Figure 8: Schematic of the radial discretization in the generalized DPI calculation.

Each ‘element’ in the discretization is defined by its distance from the well, its area, and the perimeter of its contact with the adjacent elements. Additionally, the conductivity of the fracture in each element can be calculated from a Gaussian ‘conductivity versus distance’ equation (as shown by the blue line in the right of Figure 7). The calculation can optionally incorporate fracture conductivity anisotropy. As shown in Figure 4, anisotropy causes the drainage regions to be ellipses instead of circles. If using ellipses instead of circles, the area and perimeter values in the calculations must be adjusted accordingly.

Using this radial/elliptical discretization, we perform a simple numerical flow calculation. We combine the equations for matrix linear flow and Darcy’s law for 1D flow through a fracture to calculate the inflow to a fracture element from the matrix and the pressure drop along a fracture element respectively.

For isotropic conductivity, the flow rate into the fracture is given by:

$$q_{mat, r1 \text{ to } r2} = 2\pi(r2^2 - r1^2)(P_{res} - P_f) \sqrt{\frac{\phi c_t k}{\pi \mu t}}, \quad (16)$$

and the pressure drop between adjacent fracture elements is:

$$P_{r2} - P_{r1} = \frac{q_{frac} \mu}{\pi C_{fracture}} \frac{r2 - r1}{r1 + r2}. \quad (17)$$

With anisotropy, Equations 16 and 17 are adjusted to account for the perimeter and area relationships of an ellipse.

The elements may contact different layers that have different formation properties (porosity, permeability, etc.). To account for this heterogeneity, Equation 16 can be applied separately to account for production from each layer into each element. If the system has reached boundary dominated flow, the reservoir pressure can be reduced from its ‘initial’ reservoir pressure to account for the reduction in the overall ‘average’ reservoir pressure.

The calculation starts with a known bottomhole pressure and seeks to calculate production rate as a function of known fluid and formation properties, drainage region geometry, fracture conductivity function (with respect to distance), and the cumulative duration of production up until that point in time. The calculation performs a finite difference mass balance calculation on each radial fracture ‘element,’ with a pseudosteady-state calculation that assumes ‘flow in’ equals ‘flow out.’

The fluid calculation is performed as a ‘single phase’ calculation, using a pseudophase defined from the saturated weighted average of the oil, water, and gas phase properties during production, using the procedure in Appendix 2 from Almasoodi et al. (2023).

The goal of the calculation is to assess the relative impact of interference on production (rather than the absolute magnitude), and so the ‘number of flowing fractures’ connected to each well does not need to be considered.

The procedure is:

1. Make a guess for production rate into the well (in terms of ‘reservoir volumes,’ not standard volumes). Using this flow rate and Equation 17, calculate the pressure in the radial fracture element closest to the well (adjusting for anisotropy if necessary).
2. Calculate the inflow from the matrix into the first fracture element using Equation 16 (adjusting for anisotropy if necessary).
3. For the next element, calculate its flowrate as $q_{frac,2} = q_{frac,1} - q_{mat,1}$.
4. Calculate the pressure drop along the second fracture element using $q_{frac,2}$ then calculate its drawdown by subtracting this pressure drop.
5. Repeat Steps 2-4, iterating outwards until (a) the boundaries of the discretization are reached, or (b) drawdown in the fracture element is reduced to zero (i.e., the pressure in the fracture is the same as the reservoir pressure).
6. The solve has converged when q_{frac} reaches zero in the same fracture element where pressure drawdown reaches zero (i.e., when the fracture pressure reaches the reservoir pressure). If the rate assumed in Step 1 is too low, then during the solve, an element will be encountered that has more inflow from the matrix than it has ‘outflow’ into the adjacent fracture element. As a result, the

equation in Step 3, $q_{frac,2} = q_{frac,1} - q_{mat,1}$, will yield a negative number. If the rate assumed in Step 1 is too high, then an element will be encountered where Equation 3 yields a fracture element pressure that is greater than the reservoir pressure, but q_{frac} is still positive. At the correct rate, neither of these contradictory conditions is met, and instead, q_{frac} will correctly reach zero in the same fracture element where pressure reaches the formation pressure.

7. If the solve has not converged, repeat Steps 1-5 to search for the rate (assumed in Step #1) that satisfies the convergence criterion. Once converged, convert the ‘reservoir’ volumes to ‘surface’ volumes.
8. Using the technique described in Appendix D, repeat the calculation across a population of fractures to account for heterogeneity in the conductivity of the fractures between the wells.

Step #8 (described in Appendix D) is needed because the interference test measures the most conductive fracture connection between the wells. There will likely be a distribution of conductivity values connecting the wells, and fractures with a weaker connection will experience less interference.

The generalized Degree of Production Interference from each well can be calculated by removing a well from the configuration and repeating the calculation. After a well is removed, the production of the remaining wells will increase, enabling an estimate for the DPI from that well on its neighbors. Alternatively, the calculation can be run with only a single well, and then repeated with all wells included. This calculation yields the well’s FPL – the relative amount that production is reduced at that well because of interference from its neighbors.

Figure 9 shows a summary of the Generalized Degree of Production Interference workflow described in this section.

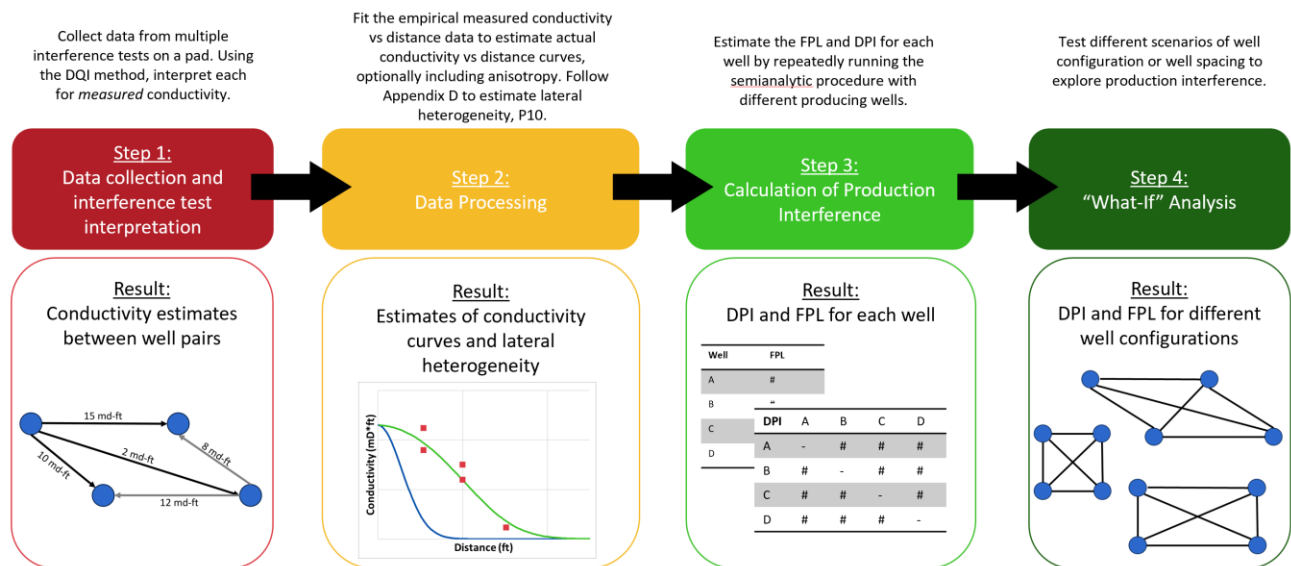


Figure 9: Summary of the workflow from interference test gathering on a pad to estimations of production interference for generic well configurations.

2.5 Numerical simulations

The simulations in this study are performed with a combined hydraulic fracturing and reservoir simulator, as described by McClure et al. (2023b). For simplicity, the fracturing stage is omitted from the simulations; they are run with one or more ‘preexisting fractures,’ and they are given uniform

conductivity. For simplicity, the simulations are run with single phase liquid. Figure 10 shows the base case simulation.

3. Results and Discussion

3.1 Do CPG values reach a long-term plateau during interference tests?

The simulation result shown in Figure 2 suggests that CPG should gradually rise to a plateau. However, it may require weeks or months to reach this plateau. This is concerning because a single value of CPG is reported for each test, and the timing of this measurement is not standardized (it is usually around 24 to 48 hours). Does this matter for CPG interpretation? When and under what conditions might we see a CPG plateau?

To investigate, we ran a series of simulations, varying conductivity and permeability. The simulations extend to 2000 hours (83 days), longer than a real-life interference test, in order to see the long-term behavior of the transient. Figure 11 shows simulations with different values of conductivity and matrix permeability of 25 nd. Figure 12 shows simulations with different values of conductivity and matrix permeability of 250 nd.

The simulations suggest that in cases with high permeability and fracture conductivity, the test reaches the long-term plateau rapidly, potentially within the 1-2 day duration of a typical interference test (lower panels of Figure 12). However, in the cases with relatively lower permeability or conductivity, CPG is likely to still be increasing after 2 days (upper left panels of Figure 11 and Figure 12). In some cases, CPG appears to plateau during an intermediate period of time (days to weeks), but then subsequently increases (Figure 11). This result suggests that even if CPG *appears* to plateau during a practical interference test, this may not represent the true long-term behavior of the system.

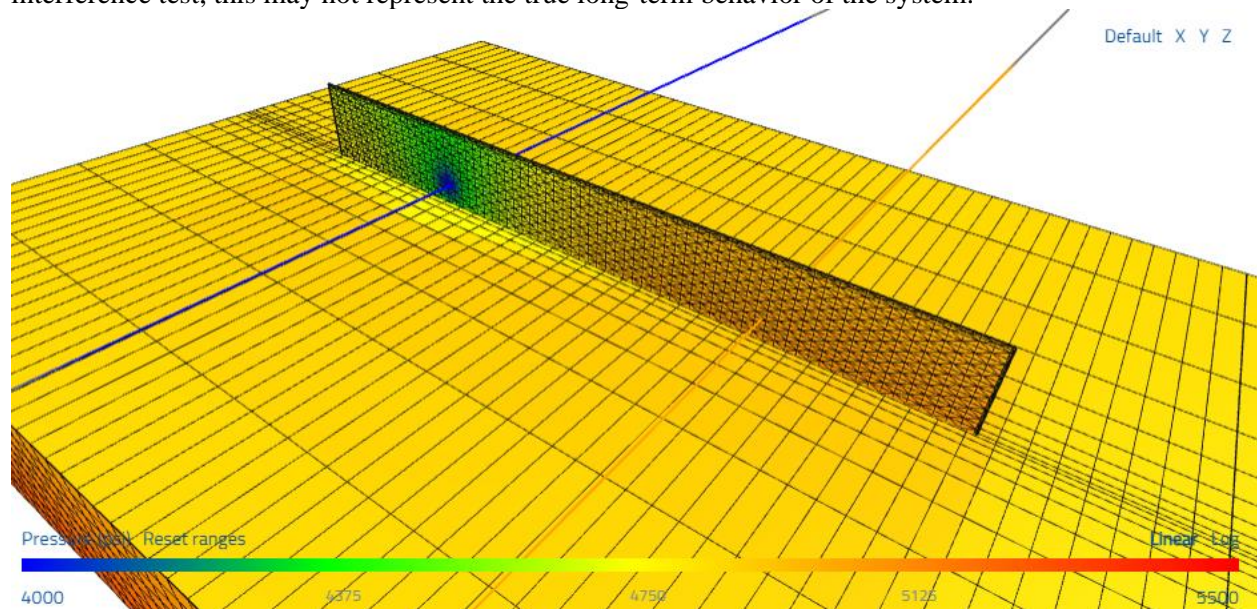


Figure 10: Problem setup for a baseline numerical simulation of an interference test. In this example, the well spacing is 880 ft.

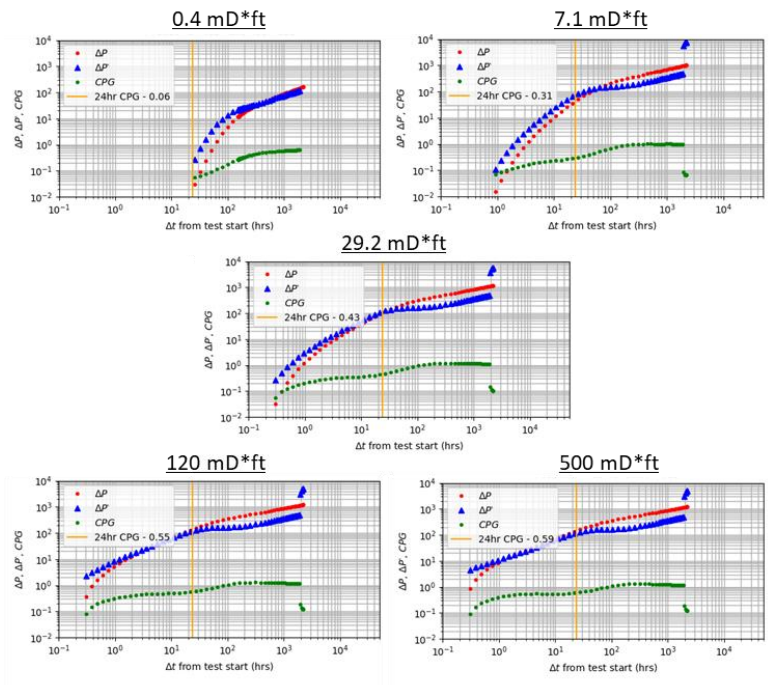


Figure 11: Simulated interference tests with fracture conductivity from 0.4 md-ft to 500 md-ft, and a matrix permeability of 25 nd. Each simulation extends to 2000 hours (83 days), significantly longer than a typical field test.

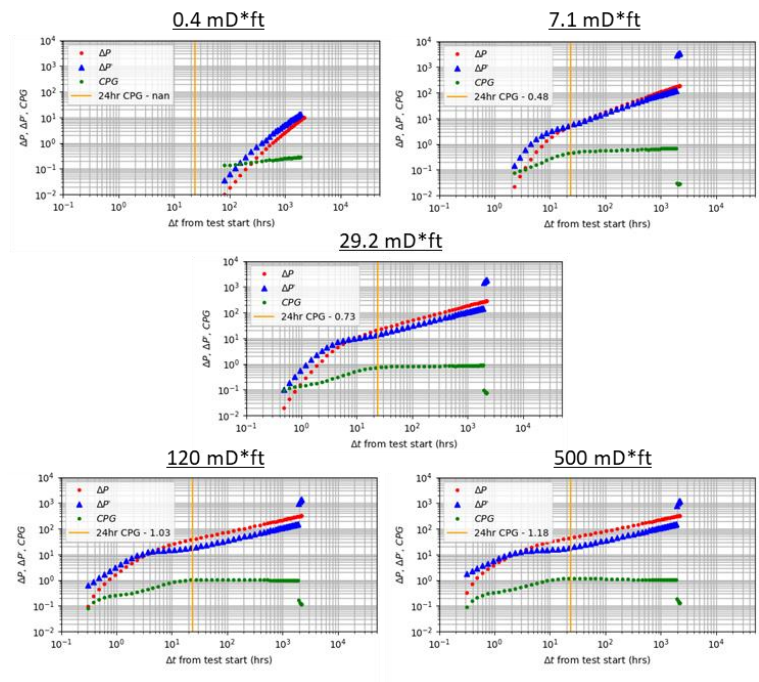


Figure 12: Simulated interference tests with fracture conductivity from 0.4 md-ft to 500 md-ft, and a matrix permeability of 250 nd. Each simulation extends to 2000 hours (83 days), significantly longer than a typical field test.

From the perspective of the production well, the transient experiences transitions in flow regime over time, such as between fracture linear, bilinear, and matrix linear (Horne, 1995). Observing these transients from the perspective of an offset monitoring well introduces an additional layer of complexity – the response observed in the monitoring well is attenuated from the response observed in the production well. The attenuation is itself changing nonlinearly over time.

We do not attempt to derive a detailed theory describing the various possible and transitions that may be observed from the perspective of the monitoring well. However, we do make a few general observations.

At the monitoring well, $\Delta P'$ is initially zero. As the impact of production begins to be felt, $\Delta P'$ increases from zero, creating a steep initial slope on the loglog plot, and then gradually flattening towards its long-term plateau. CPG is proportional to the reciprocal of the slope of the $\Delta P'$, and so because $\Delta P'$ starts steep and then flattens, CPG starts low and increases over time.

This explains why higher CPG values are associated with stronger fracture-to-fracture connection. Figure 11 and Figure 12 show that with higher fracture conductivity, the transition to the eventual ‘matrix linear flow’ regime occurs more rapidly. In turn, this causes CPG to increase from zero and reach its plateau sooner. When the conductivity is lower, CPG increases from zero later, and the increase occurs more slowly. The overall effect is that when conductivity is higher or spacing is lower, then CPG increases sooner and more rapidly. Therefore, when CPG is evaluated at a particular point in time, such as 24-48 hours, it will tend to be a larger number when the connection is stronger.

Simulations (run with slightly compressible reservoir fluid and viscosity of 0.3 cp) suggest that if permeability is greater than 100-200 nd and conductivity is greater than around 20-30 md-ft, then the long-term plateau can be reached within a few days. With lower values of permeability or conductivity, it is likely that the test will not have stabilized within a few days, or else, it may have reached a temporary plateau. With different fluid properties, these results would be different.

In actual data, do we typically observe CPG plateauing or reaching an increasing trend? The results are mixed. Figure 13 shows examples of actual field interference tests where CPG appears to plateau. Figure 14 shows field examples where CPG does not appear to plateau.

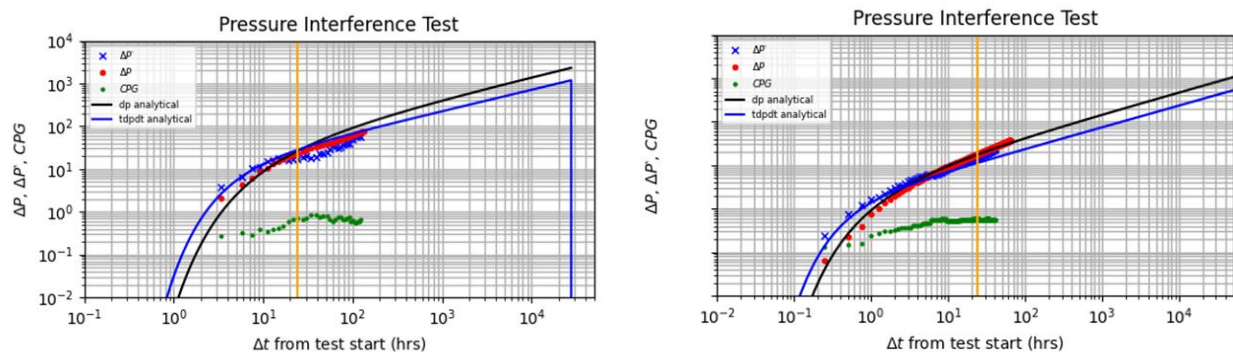


Figure 13: Field examples of interference tests with apparently plateauing CPG value.

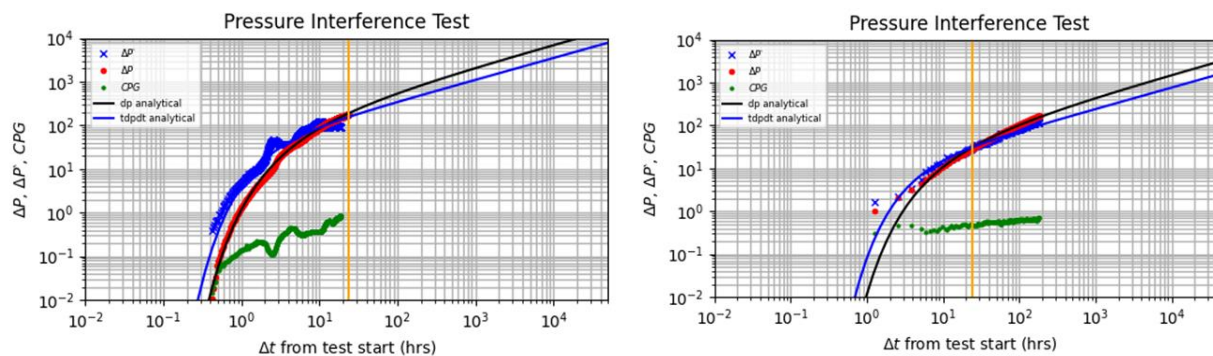


Figure 14: Field examples of interference tests where CPG does not reach a plateau.

3.2 What are possible interpretations of a long-term CPG plateau, if it occurs?

If the CPG does reach a ‘long-term’ plateau, is there any reason why it should be different from 1.0, the value that corresponds to linear flow? More generally, what is the relationship between rate-transient analysis and interference testing?

In RTA analysis, it is commonly observed that production declines more rapidly than would be expected from pure linear flow (Figure 20 from McClure et al., 2023a). In an RTA curve fit, this can manifest as a CPG value less than one (Chu et al., 2017). It is unclear whether these RTA observations – which occur over months or years of production – can be related to what is observed in an interference test – pressure drawdown observed in an offset well over a few days.

There are several possible causes of RTA deviation from linear flow. The most obvious is transition towards ‘boundary dominated flow’ as adjacent fractures experience interference from their neighbors. However, while this phenomenon is definitely occurring, it is not solely capable of explaining observed production data. Deviation from linear flow often occurs very early in the life of a well, and if we assume uniform fracture spacing, then it will be impossible to match the actual production volumes without assuming implausibly short fracture lengths and high formation permeability (Fowler et al., 2019). In contrast, field observations show that pressure depletion typically extends hundreds of feet from each well (Li et al., 2020; Cipolla et al., 2022; Benish et al., 2024).

To resolve this problem, Acuna (2020) proposes to model depleting fractures as occurring in irregularly spaced swarms. Compared with the uniform fracture spacing assumption, the Acuna (2020) model allows for an earlier, more gradual onset of fracture-to-fracture interference. This results in RTA curves that are more consistent with actual field observations (and which exhibit CPG values less than 1.0).

The mechanism proposed by Acuna (2020) could theoretically affect the CPG measurements from the interference test, just as it affects the CPG measured during long-term drawdown. To demonstrate, we simulated an interference test with D , the ‘fractal dimension,’ set to 0.6 in the simulator (see Section 19.10 from McClure et al., 2023b, for details of how the Acuna concept is implemented in the simulator). For comparison, we also ran a baseline simulation with ‘fractal dimension’ set to 0 (so that the ‘fractal fracture spacing’ mechanism is turned off and has no effect). The simulations were performed with fracture conductivity of 10 md-ft and 1000 md-ft and with a permeability of 250 nd. The result is shown in Figure 15 and Figure 16.

In the simulation with fractal dimension set to 0 and conductivity of 10 md-ft, the CPG value asymptotically approaches 1.0 (first panel of Figure 15), which is equivalent to ‘linear flow.’ In the

simulation with fractal dimension set to 0 and conductivity of 1000 md-ft, the transient progresses rapidly to reach the asymptotic value of 1.0.

When the simulations were repeated with fractal dimension set to 0.6, the transient asymptotically approached a CPG value of 0.625, instead of 1. This occurs because, at the long-term plateau, the value of a for an otherwise linear flow geometry is (pages 2 and 3 from Acuna, 2020):

$$a_{lin}(D) = 1 - \frac{1-D}{2} = \frac{1+D}{2}, \quad (18)$$

and the value of CPG is:

$$CPG_{lin}(D) = \frac{1}{1+D}. \quad (19)$$

Equation 19 shows that for D equal to 0.6, CPG at the long-term plateau should be 0.625.

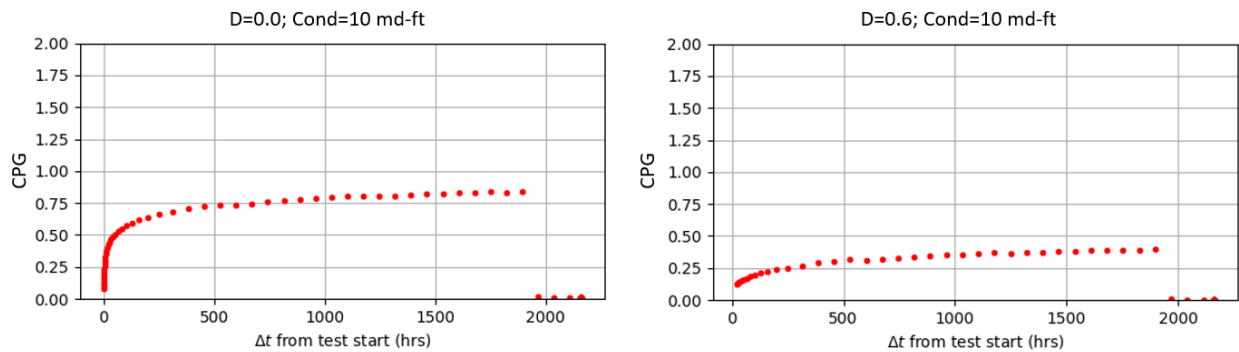


Figure 15: Interference test simulations comparing the effect of modifying 'fractal dimension' from 0 to 0.6. Both have conductivity of 10 md-ft.

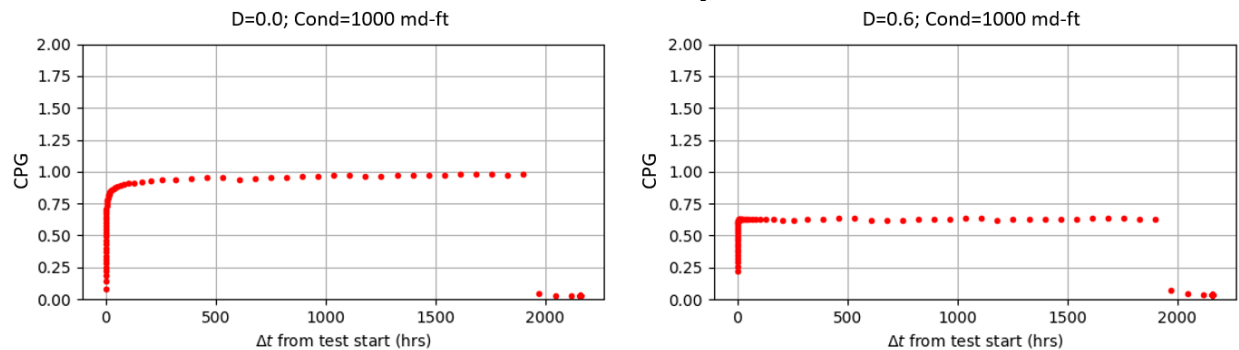


Figure 16: Interference test simulations comparing the effect of modifying 'fractal dimension' from 0 to 0.6. Both have conductivity of 1000 md-ft.

The simulations show that, if the long-term plateau is reached during the test, it is possible for the CPG value measured from an interference test to be the same as the CPG value that would be observed from RTA during long-term production.

However, there are other causes of RTA deviation from linear flow that would *not* be significant during an interference test: (a) relative permeability loss as pressure goes below the saturation pressure, (b) pressure/stress dependent fracture conductivity, (c) time-dependent fracture conductivity loss, and (d) pressure/stress dependent loss of *system permeability* around the propped fractures (Section 8.5.9 from McClure et al., 2024). These additional mechanisms cause greater deviation from linear flow (lower CPG

value observed in long-term RTA) than might be expected solely from the CPG measurement during the interference test.

Therefore, while an apparent plateau from an interference test might hypothetically be predictive of the long-term CPG value in the RTA analysis, this can only occur under specific conditions: (a) the conductivity and permeability must be sufficiently high that the test reaches its true long-term asymptote within the duration of the test, and not be affected by a temporary flattening prior to the long-term asymptote, and (b) the deviation from linear flow observed during long-term production must be caused *solely* by the Acuna (2020) fractal fracture swarm mechanism, and not by other possible mechanisms, such as relative permeability or conductivity loss. These conditions are unlikely to be satisfied in most practical applications, and so it is risky to assume that the CPG value from an interference test will be predictive of the RTA CPG value seen during long-term production.

3.3 Empirical comparison between CPG and two-well DPI

Figure 17 shows a comparison of empirically measured CPG and two-well DPI measurements from 179 interference tests in the 3 basins. The results are consistent with the simulation predictions from Almasoodi et al. (2023) – (a) there is a qualitative relationship that higher fracture conductivity is associated with larger CPG values, and (b) a CPG measurement on its own is not highly predictive of conductivity or DPI – there is a large spread in potential values. Note that the y-axes of the plots use a logarithmic scale. As shown by Almasoodi et al. (2023), the CPG has only a weak correlation with the strength of interference because among other reasons, it does not normalize for the effect of permeability and fluid properties.

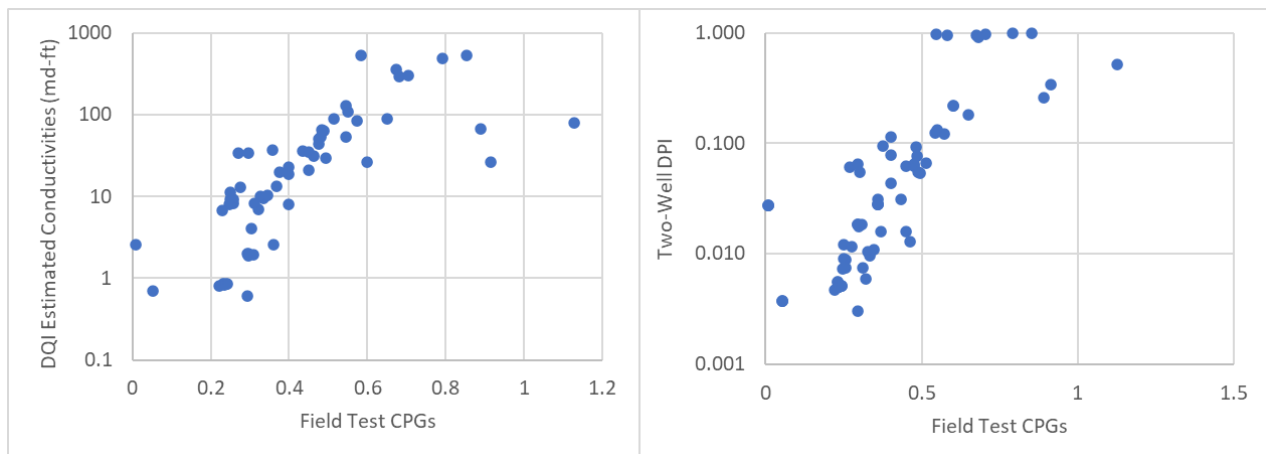


Figure 17: Comparison of empirically estimated CPG and fracture conductivity measurements from 179 field tests in the 3 basins.

3.4 Validating the generalized DPI procedure with numerical simulations

We validated the generalized DPI procedure from Section 2.4 by comparing against results from numerical simulations. Starting with the five-well configuration shown in Figure 18, we ran a series of simulations removing one or more wells from the pattern. For each scenario, we: (a) calculated the DPI directly from the numerical simulations, and (b) estimated the DPI with the fast approximate calculation in Section 2.4. For each well configuration, we ran simulations with different values of permeability, porosity, and conductivity.

The upper panels of Figure 18 show the DPI from shutting-in the four wells surrounding the middle well. The lower panels show the DPI effect on a corner well from shutting-in the middle well. The scatterplots show a very good correspondence between the results from the full numerical simulation and the results from the fast-running radial discretization method. The cases with greater DPI correspond to larger values of ‘linear flow’ dimensionless fracture conductivity (as derived by Almasoodi et al., 2023), corresponding to higher fracture conductivity and lower permeability.

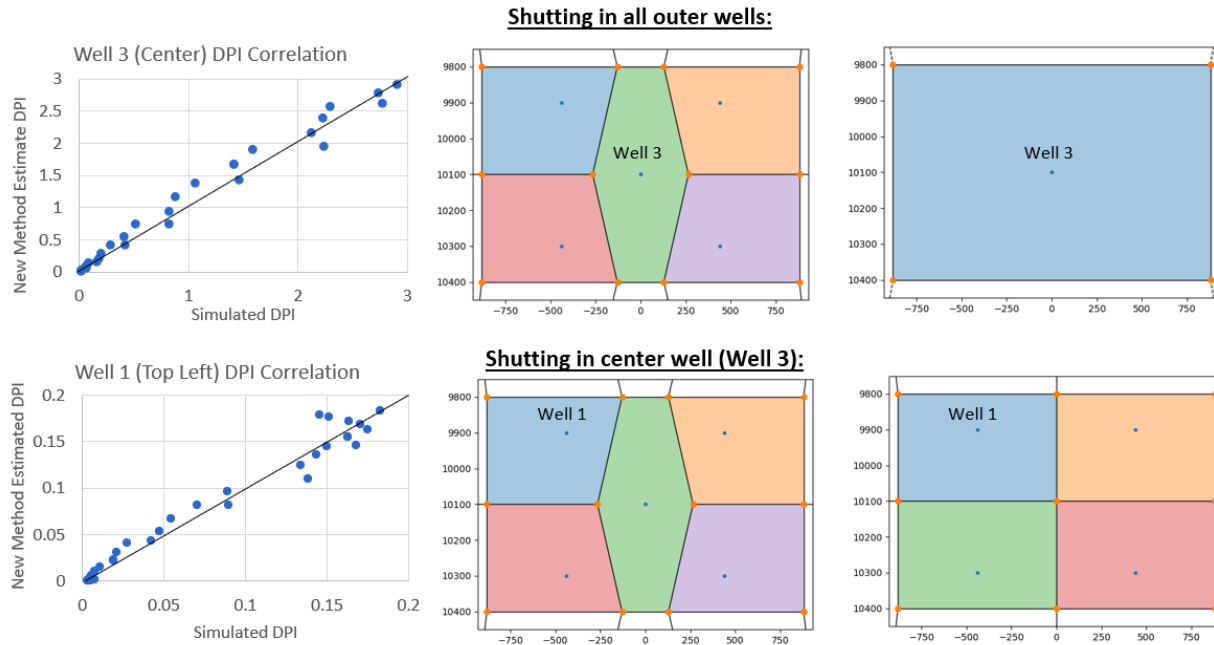


Figure 18: Comparison of DPI estimates from full numerical simulation and from the fast approximate solution. The axis scale is stretched vertically on the drainage region plots. The upper panels show the effect of shutting in all wells except Well 3. The lower panels show the effect of shutting in the center well and continuing production in the other four wells.

As shown in the upper panels, when the middle well is shut-in, there are DPI values as great as 3, corresponding to an FPL of 0.75. Production loss is large because the well is bounded on all sides, which strongly restricts production. Conversely, when only the middle well is shut-in, the largest DPI effect on each of the corner wells is near 0.2, corresponding to FPL of 17%.

3.5 Case study validating the generalized DPI procedure with field data

This case study involves a series of shut-ins across a group of wells in the Midland Basin, as shown in Figure 19. Over a series of phases, the wells were shut-in for 1-2 week periods, giving the opportunity to directly observe the impact on the production of their neighbors (i.e., directly observe the DPI). The production responses to the shut-ins are shown in Figure 20. The shut-ins were not sufficiently long to reach a stabilized value. However, extrapolating the responses forward in time, we can roughly estimate their eventual long-term plateau. While not discussed in this paper, the same combined hydraulic fracturing and reservoir simulator, as described by McClure et al. (2023b) as used to create detailed history matched model for Wells D, E, and G. This included a thorough history match of the interference tests as well as the production responses to the Phase 2 shut-ins. In this simulation, the rate deflections observed in Wells D and E plateaued at approximately 2.5x the values at the end of the Phase 2 shut-in, as

shown in the left of Figure 20. For purposes of extrapolating the field responses to estimated long-term plateaus, we scaled up the rate deflections by 2.5x.

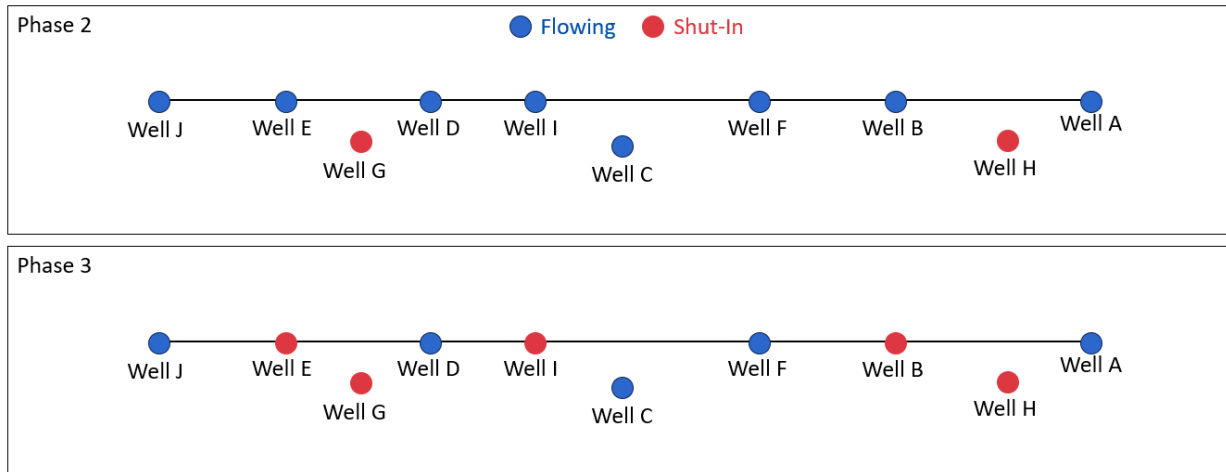


Figure 19: Gunbarrel view of the wells analyzed in the case study, as well as relevant offset wells. Prior to ‘Phase 2,’ all wells were producing. Next, Wells G and H were shut-in (upper panel). Several days later, in ‘Phase 3,’ Wells B, E, and I were also shut-in.

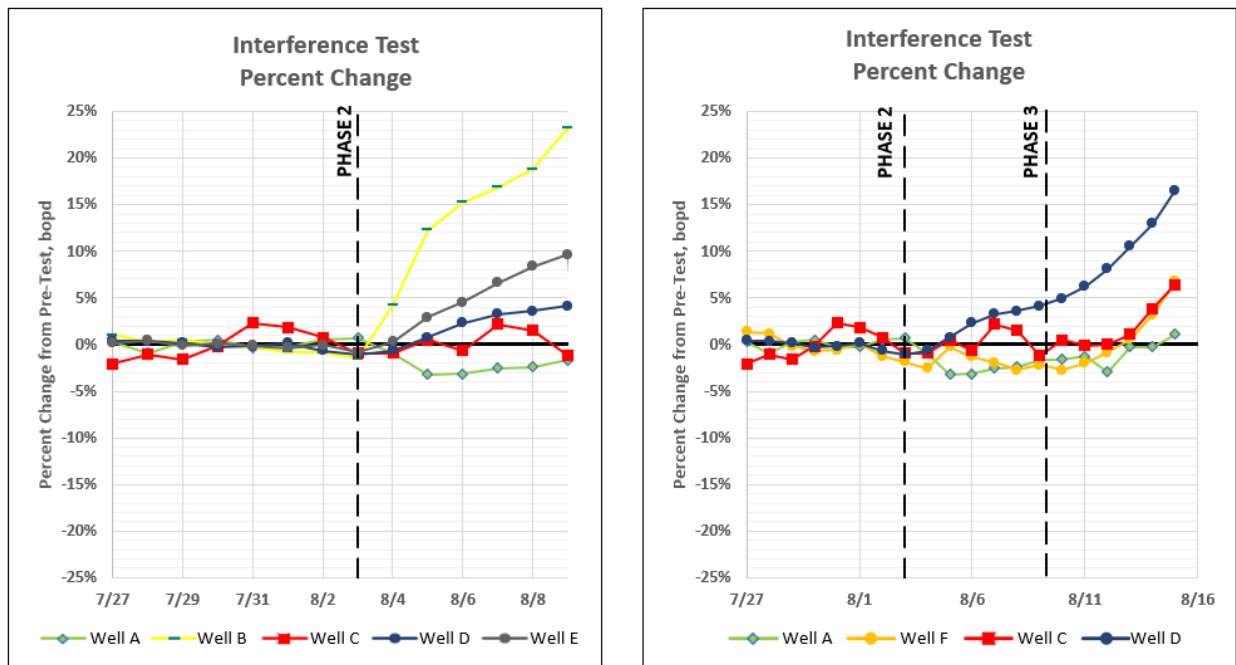


Figure 20: Field data from the case study - percent change in offset oil production after a well shut-in. The left-hand side of Figure 17 shows the percent change in production rate after the shut-in of Wells G and H (labeled ‘Phase 2’). The right-hand side of Figure 17 shows subsequent change in production rate after the shut-in of Wells B, E, and I (labeled ‘Phase 3’).

After the shut-ins, the wells were put back on production, creating a series of interference tests. For example, Figure 21 shows two of the interference tests – the effect of production in Well B on Well A and Well F.

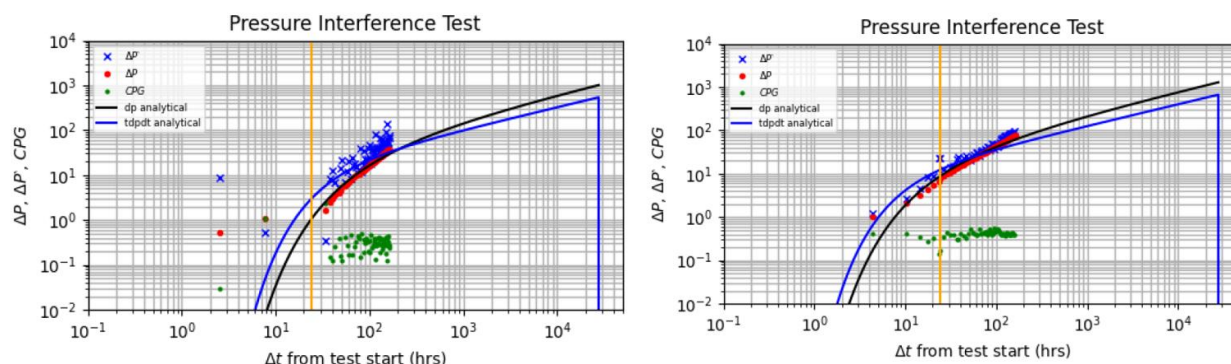


Figure 21: Pressure measurements at wells A and F when Well B was put on production.

The left panel of Figure 22 shows an aggregation of all the interference tests in the dataset. The plot has two curves – the conductivity ‘as-measured,’ and the implied ‘true’ conductivity versus distance (as discussed in Section 2.4). Overall, the results have a fair amount of scatter, but are sufficient to define a general trend in conductivity versus distance.

The final step is to approximate the heterogeneity that exists between the fractures along each well. As discussed in Section 2.4, the DQI method measures the most conductive fracture connection between each pair of wells. Many or most other fracture connections will have significantly lower conductivity. To account for this heterogeneity, we postulate that the distribution of conductivity values around the well can be described by Equation D1. The equation is parameterized by the parameter p_{10} , where larger values of p_{10} suggest greater heterogeneity. The value of C_0 in Equation D1 is determined from the ‘actual’ conductivity versus distance curve, as shown in the left panel of Figure 22. The value of p_{10} can be estimated from production history matching, as outlined in Appendix D. We chose to use the same value of p_{10} for every well in the dataset. The ‘best fit’ value of p_{10} for all wells in the dataset was found to be 0.28. The right panel of Figure 22 shows the distribution of conductivities from the ‘best fit’ distribution. The total number of fractures was assumed to be 90% the number of perforation clusters.

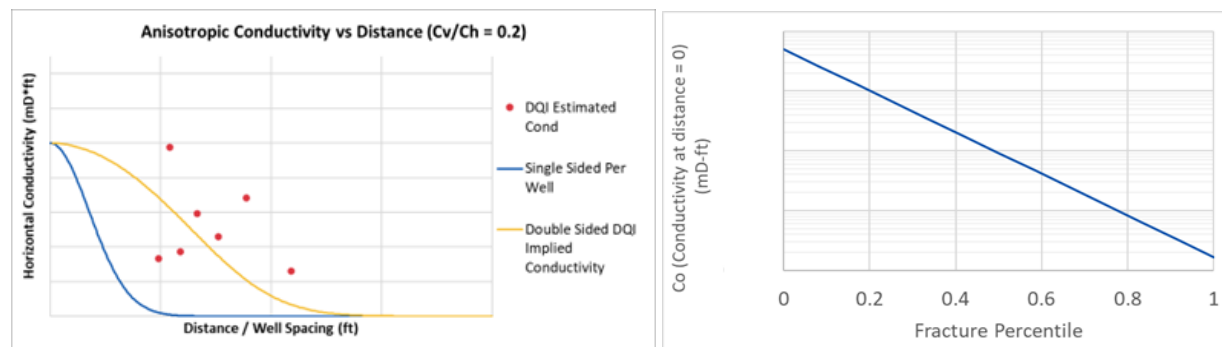


Figure 22: DQI estimated conductivity versus well spacing for the various interference tests (red) with Gaussian fit (yellow); derived horizontal conductivity vs distance from well (blue). Horizontal conductivity is 5x greater than vertical conductivity.

Using the relationships in Figure 22, we apply the generalized DPI method to predict the production responses for the wells shown in Figure 20. Figure 23 shows a cross-plot of ‘estimated stabilized DPI’

from Figure 18 versus the DPI predictions from the generalized DPI method. There is reasonably good correspondence.

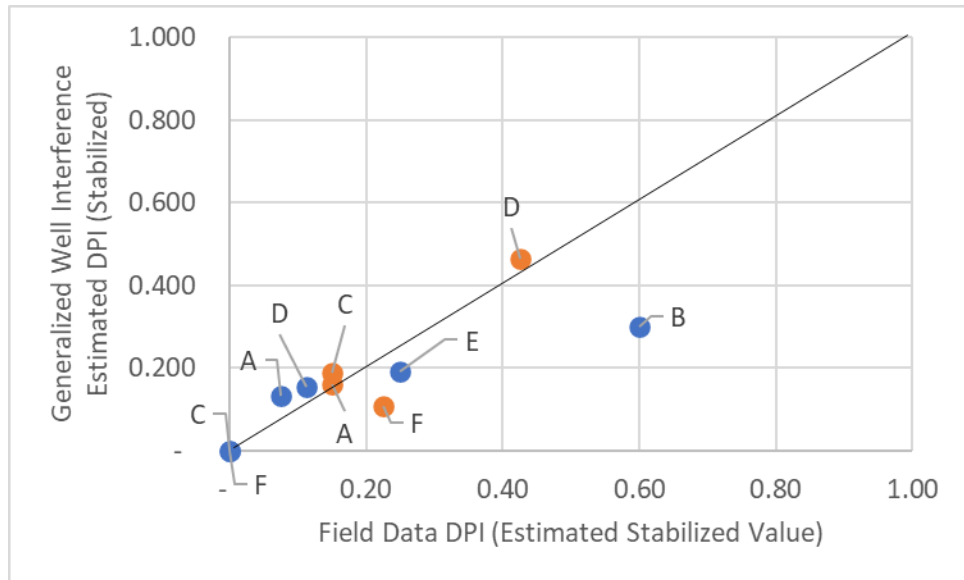


Figure 23: Cross-plot of the ‘estimated stabilized DPI’ from Figure 20 versus the DPI predictions from the generalized DPI method. Blue dots represent data points from the Phase 2 shut-ins; orange dots are from the Phase 3 shut-ins.

In Phase 2, Wells E, D, B, and A were directly offset the two wells that were shut-in. Figure 20 shows that the responses of these wells had significant variability. Well A had the least production impact, which is explainable because it is an ‘outer’ well, and so relatively less affected by production from its bounding neighbor on the other side. In Phase 3, Well D had the greatest increase in production, which is explainable because all of its surrounding wells were shut-in. However, much of the variance in well performance is not explainable, at least within the context of the analysis performed in this case study. For example, this workflow underestimates the production impact to Well B when Well H is shut-in (outlier labeled 'B' in the right of Figure 23). As the well with the largest production impact, the extrapolation from the field data to ‘stabilized’ values may be overestimating the production impact on this well. Alternatively, Well B was notably producing at a slightly lower BHP than the surrounding wells; this might have caused the estimates from generalized DPI to be low, since the workflow currently assumes equal depletion for all wells. The comparison shows the capabilities and limits of the workflow: it can capture overall trends but cannot capture the full range of variability seen in real data.

Having built the generalized DPI model, it can be used to evaluate alternative well configurations – different spacings, landing depths, etc. The generalized DPI cannot account for the full variety of real-life factors that affect production, such as differences in fracture design, sequencing, artificial lift, well construction, etc. Nevertheless, it provides a fast, practical procedure for integrating results from interference tests, inferring key physical parameters, and quantifying the effect of changing well configuration.

4. Conclusions

The results show that the CPG has a qualitative relationship with the strength of production interference because: (a) the Bourdet derivative on the loglog plot starts steep and flattens over time, (b) CPG is

proportional to the inverse of the loglog slope of the Bourdet derivative, and so it starts low and increases over time, and (c) higher conductivity and lower spacing cause the CPG increase to occur earlier and more rapidly. Therefore, as long as CPG values from different tests are compared from roughly similar points in time, higher conductivity and lower spacing will result in a higher reported CPG value.

Often, CPG appears to plateau before the end of the test. Does the CPG at this plateau have physical significance? Simulations suggest that in many cases, the plateau is only temporary. If the test had been performed for longer, CPG may have subsequently risen further. However, with sufficient fracture conductivity and permeability, simulations suggest that it is possible for a ‘long-term’ plateau in CPG to be reached within the duration of a test (usually, a few days). Under standard assumptions, we would expect this plateau to occur at a CPG of 1.0, corresponding to linear flow. If the fractures exhibit the ‘fractal fracture spacing’ mechanisms postulated by Acuna (2020), this could cause a long-term plateau at CPG less than 1.0. Even if so, we would not necessarily expect the RTA trend during long-term production to follow a similar CPG value – there are other possible causes of deviation from the ideal linear flow trend (such as relative permeability loss or conductivity loss), which would not be apparent during an interference test.

Almasoodi et al. (2023) found that the CPG metric has only a qualitative association with the strength of production interference because it does not rigorously account for differences in parameters such as: (a) fluid viscosity and compressibility, and (b) system permeability. Almasoodi et al. (2023) proposed a procedure for deriving a ‘two-well’ DPI parameter to quantify the production impact between wells. However, this parameter is only valid for the special case of two wells, unbounded on either side. In Appendix B, we generalize the procedure from Almasoodi et al. (2023) to derive a ‘uniform-spacing’ DPI that is valid for a well bounded on both sides.

We develop a procedure for calculating DPI with arbitrary wellbore configurations, accounting for: (a) the decrease in conductivity with distance, (b) arbitrary wellbore configurations, (c) anisotropy in conductivity, and (d) nonuniformity in fracture conductivity. We test the new generalized DPI procedure in a field case study that has unusually long shut-ins (useful for validation) and find that it has good predictivity.

The generalized DPI procedure can be used to run rapid ‘what-if’ analysis to evaluate the economic effect of alternative gun barrel configurations.

Acknowledgements

We gratefully acknowledge the support and collaboration of Apache, ConocoPhillips, ExxonMobil, and Hess.

Nomenclature

C: Fracture conductivity, md-ft

CPG: Chow Pressure Group, defined in Equations 2 and 7

DPI: The ‘degree of production interference,’ defined in Equation 12

DPI_{2w}: The DPI specifically for a two-well configuration

DPI_{unif} : The DPI specifically for a uniform-spacing well configuration

DQI : The ‘Devon Quantification of Interference’ method, described by Almasoodi et al. (2023)

FPL : Fractional production loss, defined in Equation 13

FPL_{2w} : The FPL specifically for a two-well configuration

FPL_{unif} : The FPL specifically for a uniform-spacing well configuration

K : Lumped parameter in the equation for 1D pressure diffusion, defined in Equation 10, md-ft²/cp

L : Characteristic length scale for depletion, defined in Equation A1, ft

L_D : Dimensionless depletion length, defined in Equation A2, ft

p_{10} : Parameter expressing the nonuniformity of the fractures along the wells, defined in Equation D1

r_{inv} : Radius of investigation, defined in Equation 11, ft

α : Hydraulic diffusivity, ft²/s

References

- Acuna, Jorge. 2020. Rate transient analysis of fracture swarm fractal networks. Paper URTeC-2118 presented at the Unconventional Resources Technology Conference, Austin, TX.
- Almasoodi, Mouin, Thad Andrews, Curtis Johnston, Ankush Singh, and Mark McClure. 2023. A new method for interpreting well-to-well interference tests and quantifying the magnitude of production impact: theory and applications in a multi-basin case study. *Geomechanics and Geophysics for Geo-Energy and Geo-Resources* 9.
- Benish, T. G., J. S Brown, S. S. Chhatre, K. K. Decker, J. D. Habrial, R. Manchanda, A. Solomou, and D. S. Vice. 2024. Evaluation of Completion Designs and Fracture Heterogeneity via an Instrumented Slant Monitor Well. SPE-217825-MS. Paper presented at the SPE Hydraulic Fracturing Technology Conference, The Woodlands, TX.
- Chu, W., N. Pandya, R. W. Flumerfelt, and C. Chen. 2017. Rate-transient analysis based on power-law behavior for Permian Wells. SPE-187180-MS. Paper presented at the SPE Annual Technical Conference and Exhibition, San Antonio, TX.
- Chu, W. C., Scott, K. D., Flumerfelt, R., Chen, C., & Zuber, M. D. (2020). A New Technique for Quantifying Pressure Interference in Fractured Horizontal Shale Wells. *SPE Reservoir Evaluation & Engineering*, 23(01), 143–157.
- Cipolla, Craig, Jennifer Wolters, Michael McKimmy, Carlos Miranda, Stephanie Hari-Roy, Aicha Kechemir, and Nupur Gupta. 2022. Observation lateral project: Direct measurement of far-field drainage. SPE-209164-MS. Paper presented at the Hydraulic Fracturing Technology Conference and Exhibition, The Woodlands, TX.
- Craig, D. P., T. Hoang, H. Li, J. Magness, C. Ginn, V. Auzias. 2021. Defining Hydraulic Fracture Geometry Using Image Logs Recorded in the Laterals of Horizontal Infill Wells. Paper URTeC-5031-MS presented at the Unconventional Resources Technology Conference, Houston, TX. <https://doi.org/10.15530/urtec-2021-5031>.

Fowler, Garrett, Mark McClure, and Craig Cipolla. 2019. A Utica case study: the impact of permeability estimates on history matching, fracture length, and well spacing. SPE-195980-MS. Paper presented at the SPE Annual Technical Conference and Exhibition, Calgary, Alberta.

Horne, Roland N. 1995. Modern Well Test Analysis: A Computer-Aided Approach, 2nd edition. Palo Alto, CA, Petroway, Inc.

Kim, Tae Hyung. 2019. Improvement of reservoir management efficiency using stochastic capacitance resistance model. Paper SPE-195322-MS presented at the SPE Western Regional Meeting, San Jose, CA.

Li, T., Chu, W., & Leonard, P. A. (2020). Analysis and interpretations of pressure data from the hydraulic fracturing test site (HFTS). SPE/AAPG/SEG Unconventional Resources Technology Conference 2020, URTeC 2020. <https://doi.org/10.15530/URTEC-2019-233>

McClure, Mark, M.L. Albrecht, C. Bernet, C.L. Cipolla, K. Etcheverry, G. Fowler, A. Fuhr, A. Gherabati, M. Johnston, P. Kaufman, M. Mackay, M.P. McKimmy, C. Miranda, C. Molina, C.G. Ponnors, D.R. Ratcliff, J. Rondon, A. Singh, R. Sinha, A. Sung, J. Xu, J. Yeo, and R.B. Zinselmeyer. 2023a. Results from a Collaborative Industry Study on Parent/Child Interactions. SPE-212321-MS. Paper presented at the SPE Hydraulic Fracturing Technology Conference and Exhibition, The Woodlands, TX.

McClure, M., Kang, C., Hewson, C., Medam, S., Dontsov, E., and Singh, A. (2023b). ResFrac Technical Writeup. <http://arxiv.org/abs/1804.02092>.

McClure, Mark, Garrett Fowler, Chris Hewson, and Charles Kang. 2024. The A to Z Guide to Accelerating Continuous Improvement with ResFrac. <https://arxiv.org/abs/2205.14820>.

Appendix A – The Almasoodi et al. (2023) procedure for deriving the two-well DPI

During depletion in shale, the propped fracture is finite conductivity, with a spatial gradient in pressure towards the producing well. From Darcy's law, the slope of the pressure gradient depends on the flow rate along the fracture and the conductivity. In turn, the flow rate depends on the rate of inflow from the formation and the position along the fracture. Near the well, flow rate is greater because of the accumulated inflow from the fracture surface area upstream.

Based on simple scaling arguments, Almasoodi et al. (2023) defined a characteristic length-scale for the length of the depleted region along the fracture:

$$L = \frac{(C_{fracture})\left(\frac{k_r}{\mu}\right)_{frac,t}}{\sqrt{2 \sqrt{\frac{\phi C_t k}{\pi} \left(\frac{k_r}{\mu}\right)_{mat,t}} t^{-0.5}}}, \quad (A1)$$

Where:

$\left(\frac{k_r}{\mu}\right)_{frac,t}$ = the total mobility of the fluid in the fracture during production,

$\left(\frac{k_r}{\mu}\right)_{mat,t}$ = the total mobility of the fluid in the matrix during production,

and the total mobility is equal to $\frac{k_{rw}}{\mu_w} + \frac{k_{ro}}{\mu_o} + \frac{k_{rg}}{\mu_g}$.

When calculating C from hydraulic diffusivity using Equation 9 (as explained in Section 2.3), the fluid properties should be consistent with the fluid in the fracture during the test (which may be water, if it is performed when the well is first put on production). However, the fluid properties in the fracture used in

the calculation of L should be representative of the fluid that will be in the fracture and formation *during long-term production*, since this scaling relates to the production impact during long-term depletion.

Using this characteristic length scale, a dimensionless drainage length, L_D , can be calculated by dividing by the half-well spacing, $0.5y$. If L_D is smaller, this implies that the drainage distance is relatively small, compared with the well spacing, which implies a smaller DPI.

$$L_D = \frac{L}{0.5y} \quad (\text{A2})$$

Running a variety of numerical simulations under different conditions, Almasoodi et al. (2023) found that all simulation collapsed onto a single curve relating L_D to the two-well DPI. The result is shown in Figure 24.

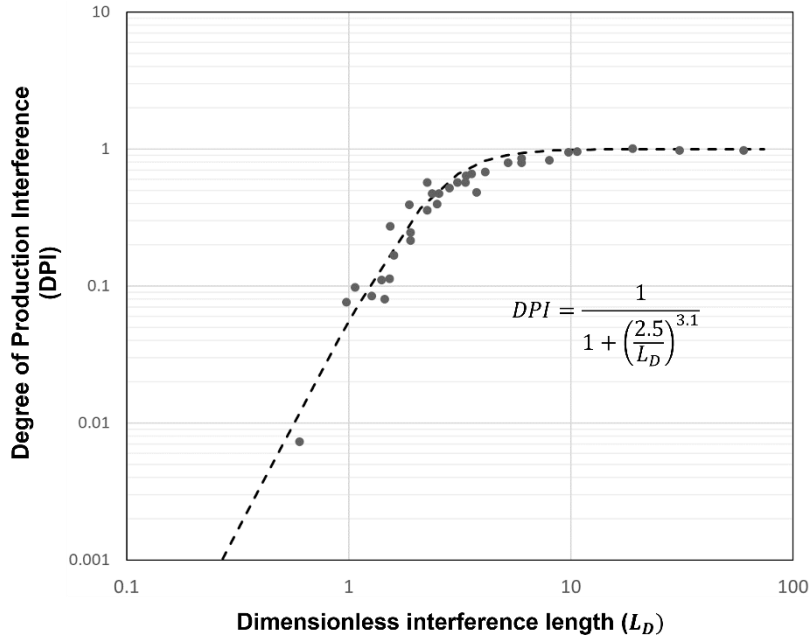


Figure 24: The relationship between L_D at two-well DPI. Figure reproduced from Almasoodi et al. (2023).

Appendix B – Derivation of the Uniform-Spacing DPI

Almasoodi et al. (2023) developed a procedure for estimating the ‘two-well’ DPI – valid for two wells, unbounded on the outside. In this section, we derive the DPI metric for wells with ‘uniform-spacing.’ In other words, for a well with neighbors on *either side*, what is the production impact from the offset wells?

Define U as the amount of production coming from one side of a well, which is unbounded on that side. Define B as the amount of production coming from one side of the well, with a producing offset well on that side. In that case, following the definitions from Equation 12, q_{20day} is equal to $U + U$, and q_{prior} is equal to $U + B$. Therefore, we can write:

$$DPI_{2w} = \frac{q_{20days} - q_{bef}}{q_{bef}} = \frac{(U+U) - (U+B)}{U+B} = \frac{U-B}{U+B} \quad (\text{B1})$$

where DPI_{2w} is the two-well DPI derived from the Almasoodi et al. (2023) procedure.

This equation can be rearranged to write:

$$U = B \frac{1+DPI_{2w}}{1-DPI_{2w}}. \quad (B2)$$

Now, let's assume that the well is bounded on both sides. Therefore, q_{prior} is equal to $B + B$.

$$DPI_{unif} = \frac{(U+U)-(B+B)}{B+B} = \frac{U-B}{B}, \quad (B3)$$

where DPI_{unif} is the DPI for a well bounded on both sides.

We can substitute Equation B2 into Equation B3 to write DPI_{unif} in terms of DPI_{2w} :

$$DPI_{unif} = \frac{U-B}{B} = \frac{U}{B} - 1 = \frac{1+DPI_{2w}}{1-DPI_{2w}} - 1. \quad (B4)$$

Thus, to calculate the uniform-spacing DPI, it is sufficient to calculate the two-well DPI from the Almasoodi et al. (2023) procedure, and then plug into Equation B4.

From Equation 14, we can combine with Equation B4 to write the expression for FPL at uniform spacing:

$$FPL_{unif} = \frac{DPI_{unif}}{DPI_{unif}+1} = \frac{\frac{1+DPI_{2w}-1}{1-DPI_{2w}}}{\frac{1+DPI_{2w}-1}{1-DPI_{2w}}+1} = 1 - \frac{1-DPI_{2w}}{1+DPI_{2w}}. \quad (B5)$$

Appendix C – Adjusting the estimated conductivity to account for anisotropy

The conductivity estimate from interference tests can be adjusted for anisotropy by multiplying by the following factor:

$$C_h = C_{estimated} \frac{\Delta x^2 + \frac{C_h}{C_v} \Delta z^2}{\Delta x^2 + \Delta z^2} \quad (C1)$$

For example, let's assume $C_{estimated}$ (the conductivity estimated from the DQI procedure described in Section 2.3) is equal to 10 md-ft. Conductivity anisotropy is 5x. The wells are laterally offset by 600 ft, and vertically offset by 200 ft. Then, C_h is 14 md-ft, and C_v is 2.8 md-ft.

Equation C1 scales Δz with the square root of the conductivity anisotropy. This scaling arises because the DPI method estimates conductivity from the early-time pressure response, and the radius of investigation scales with the square root of fracture conductivity.

Appendix D – Accounting for heterogeneity in fracture conductivity

The conductivity measured in the interference test is representative of the fracture(s) with the *strongest* connection(s) between the wells. In reality, some fractures will have lower conductivity than others, and some fractures will not connect across all wells. This has implications for the DPI estimation: wells with many strong connections will experience different production interference than wells with few strong connections.

We investigated whether we could use production data to constrain the uniformity in fracture conductivity. Consider a well with 500 fractures and an estimated fracture conductivity of 50 md-ft. The initial production rates for that well if all 500 fractures have a conductivity of 50 md-ft will be much greater than if only one fracture has conductivity of 50 md-ft with the remainder having a conductivity of 1 md-ft.

Using this concept, we can run a simplified model to estimate a parameter related to the uniformity of fracture conductivity, if we assume: (a) the number of flowing fractures per well, (b) that the *most* conductive fractures follow the conductivity versus distance function estimated using the procedure above, and (c) that the distribution of conductivity across the population of flowing fractures follows a statistical distribution that can be parameterized with a single value.

For the distribution of conductivity values, we can assume an exponential decline relation with y-intercept equal to C_0 , the conductivity of the most conductive fracture, as measured by the interference test. Assume there are N_{tot} total fractures, and that they are ordered from the most conductive fracture ($N = 1$) to the least ($N = N_{tot}$). The conductivity of fracture N can be written as:

$$C(N) = C_0 * 10^{-\frac{1}{p_{10}} \frac{N-1}{N_{tot}}}, \quad (D1)$$

where the parameter p_{10} controls the magnitude of nonuniformity. For example, if p_{10} is set to 0.6, then 60% of the fractures have conductivity within a factor of 10x of C_0 and 40% have conductivity less than 10x lower than C_0 . In the limiting cases, if p_{10} is near zero, then there is only one flowing fracture; if p_{10} is very large, then all the fractures have conductivity of C_0 .

We can now use the Generalized DPI procedure described in Section 2.4 to estimate the value of p_{10} . We need to start with an estimate of the total number of flowing fractures, N_{tot} . For a ‘typical’ well, it is reasonable to assume that number of significantly flowing propped fractures is equal to ballpark 75% of the number of perforation clusters.

To estimate p_{10} , the following procedure is employed:

1. Make an initial guess for p_{10} .
2. Using Equation D1, calculate conductivity values for all fractures, 1 to N_{tot} .
3. Perform the fast approximate flow calculation from Section 2.4 to calculate the flow rate into each fracture. Sum up their flow rate to calculate the total calculated production rate.
4. Compare the calculated production with actual. If they are close, then the calculation has converged. If not, then update the value of p_{10} and repeat.

We validated this workflow by comparing against results from a series of full numerical simulations in which fracture conductivities were assigned stochastically with a variety of different distributions. A visual example of one of the simulations is shown below along with the results of the workflow for a selection of four distributions. In this chart, the dots represent the actual fracture conductivities versus percentile set up in the simulations. The lines represent the ‘fit’ curve estimated by the rate-match process just described.

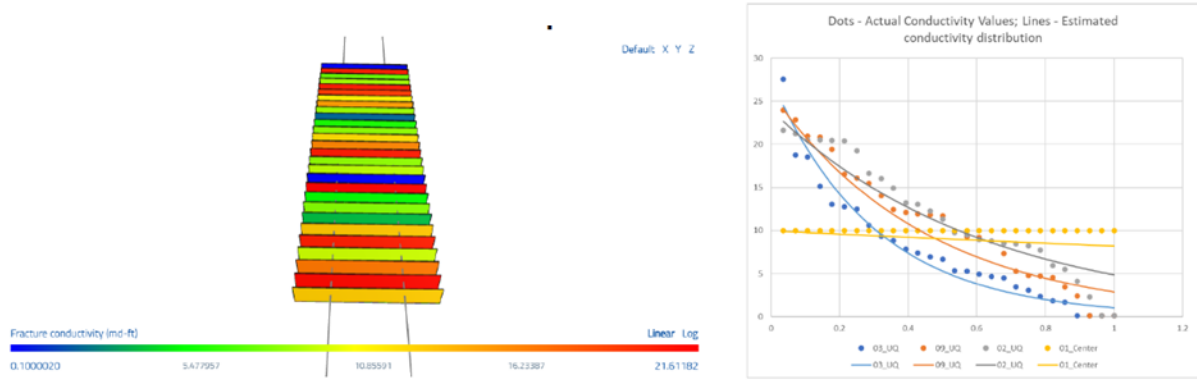


Figure 25: Numerical simulation set-up used to validate the procedure for accounting for fracture conductivity heterogeneity.